A Novel Sensorless Photovoltaic Power Reserve Control With Simple Real-Time MPP Estimation

Xingshuo Li, *Student Member, IEEE,* Huiqing Wen, *Senior Member, IEEE,* Yinxiao Zhu, Lin Jiang, *Senior Member, IEEE,* Yihua Hu, *Senior Member, IEEE,* Weidong Xiao, *Senior Member, IEEE,*

Abstract

Power reserve control (PRC) without energy storage becomes essential for modern photovoltaic (PV) power plants to meet the increased ancillary service requirements such as grid frequency support. Conventional PRC strategies show obvious limitations to estimate the available maximum power point (P_{avai}), such as additional hardware requirements, implementation difficulty and slow estimation speed. Originated from the linear characteristic of PV curves in the constant current region (CCR) and a Lambert-W function for voltage linear reference, P_{avai} is estimated separately in separate steps rather directly measured or estimated. The proposed strategy does not requires any additional hardware such as the irradiance and temperature sensors, which realizes sensorless control with reduced cost. Furthermore, cumbersome procedures of curve fitting with sophisticated operating points sampling and key parameters determination in the real-time P_{avai} estimation by using the conventional PRC methods can be also eliminated. In this strategy, the operating point with a curtailed power level is allocated at the left-hand side of the MPP, which guarantees the stability of PV systems under varying conditions. The developed strategy exhibits fast speed to estimate P_{avai}, high robustness, and good compatibility with existing PV systems. Simulation and experimental results under various scenarios are provided to validate the effectiveness of the proposed strategy.

Index Terms

Active power control (APC), Power reserve control (PRC), Maximum power point tracking (MPP-T),Power Curtailment, Grid Frequency Support, Photovoltaic (PV).

I. Introduction

In recent years, PV systems have been increasingly integrated into the power grid [1]. As the penetration level of PV systems increases, a large number of conventional power plants will be replaced by the PV power plants [2]. As a consequence, the overall system inertia and the power reserved and provided for the primary and secondary control will be reduced [3–5]. Therefore, the Rate of Change of Frequency (RoCoF) and the frequency deviation of the power system will be affected and consequently lead to critical frequency stability problems [6].

In order to overcome the frequency stability problems, grid regulations and network codes are continuously revised to deal with the intermittent nature of PV power and grid security [7]. Therefore, power reserve control (PRC) in PV systems is required to take part in the system frequency regulation. Usually this PRC can be realised by two methods: providing energy storage devices or power curtailment [8]. The former normally uses batteries to realise the power reserve [9–11]. However, the drawbacks of this method is high initial investment and limited lifetime. Besides, integrating batteries into PV systems also increase the overall system cost and complexity, which is not so cost effective [12].

Alternatively, the power curtailment method is much simpler, lower implementation cost and easier to be adopted in the current power system [13–17]. The basic idea of this method is the PV systems working at a suboptimal power level rather the maximum power of PV panels by modifying the maximum power point tracking (MPPT) techniques, and then the active power can be reserved in order to realise potential grid support. Furthermore, the concept of the power curtailment method is also used for other utility scale technology [18], such as constant power generation control (CPGC) [19–21] and power ramp-rate control (PRRC) [22–26]. Although the main concern of this method is associated with energy loss caused by the curtailed PV power [27], the reduction of the energy can also reduce the thermal loading of switching devices. Consequently, the inverter lifetime can be increased as a compensation [28].

Fig. 1 shows the basic concept and typical curves of PV panels with the PRC. As shown in Fig. 1, the PV power P_{pv} is regulated at the curtailed level P_{limit}, which can be calculated as:

$$P_{pv} = P_{limit} = P_{avai} - \Delta P \tag{1}$$

where P_{avai} refers to the maximum available power and ΔP refers to the required amount of reserved power. Generally, ΔP is determined by the system operator. P_{avai} is affected by the weather conditions such as solar irradiance and temperature, thus, fast and effectively estimating P_{avai}, tracking P_{limit} and maintaining ΔP at a certain level under dynamic conditions is the key issue [29].

Many methods for the determination of the available power, P_{avai}, have been proposed and can

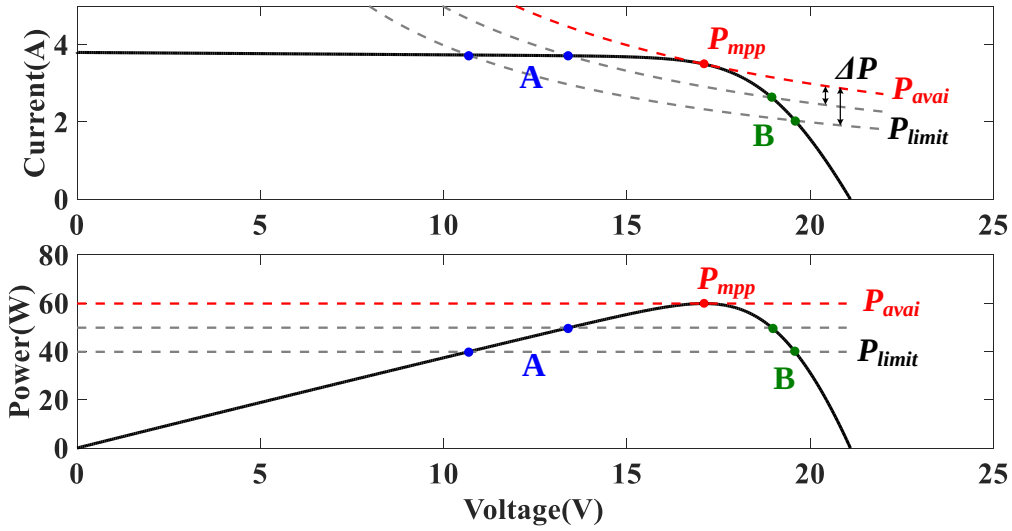

Fig. 1. I-V and P-V characteristic curves with the operating point at the curtailed level P_{limit}.

be categorized into two categories: measurement based methods and curve-fitting based methods. The former category, as shown in Fig. 2 (a)-(c), P_{avai} is measured rather than estimated. Besides, most of them have additional hardware requirements. In [30, 31], combined with the PV array characteristic model, an accurate measurement of the solar irradiance and temperature is required to calculate P_{avai}. As shown in Fig. 2 (a), the off-line calculation is used to estimate the parameters of PV string, and then, P_{avai} is calculated from the solar irradiance and temperature measurement in real time. This method is straightforward and very effective to estimate P_{avai}. However, additional sensors required for the solar irradiance and temperature measurement will increase the cost and complexity of the whole system. In [32], the system periodically enters the fractional open-circuit voltage MPPT mode to estimate P_{avai}. As shown in Fig. 2 (b), the power at $80\%V_{oc}$ can be approximately regarded as P_{avai}. Once P_{avai} is measured, this method perturbs the operating point until reaches the curtailed power P_{limit}. Since the dc-link capacitors will buffer the PV power increase during the MPPT operation for the P_{avai} estimation, the dc-link voltage is increased, which may raise over-voltage concern without proper control. In [33], a coordinated control strategy is proposed for PV strings in a master-slave mode. It assumes that two PV strings have similar solar irradiance and temperature profiles since they are located close to each other. As shown in Fig. 2 (c), the master PV string uses the MPPT algorithm to track its MPP while the slave PV string directly utilizes the tracked MPP result as its P_{avai}. This method can realize the accurate regulation of the reserved power and ensure the stable operation. However, the two PV systems have to

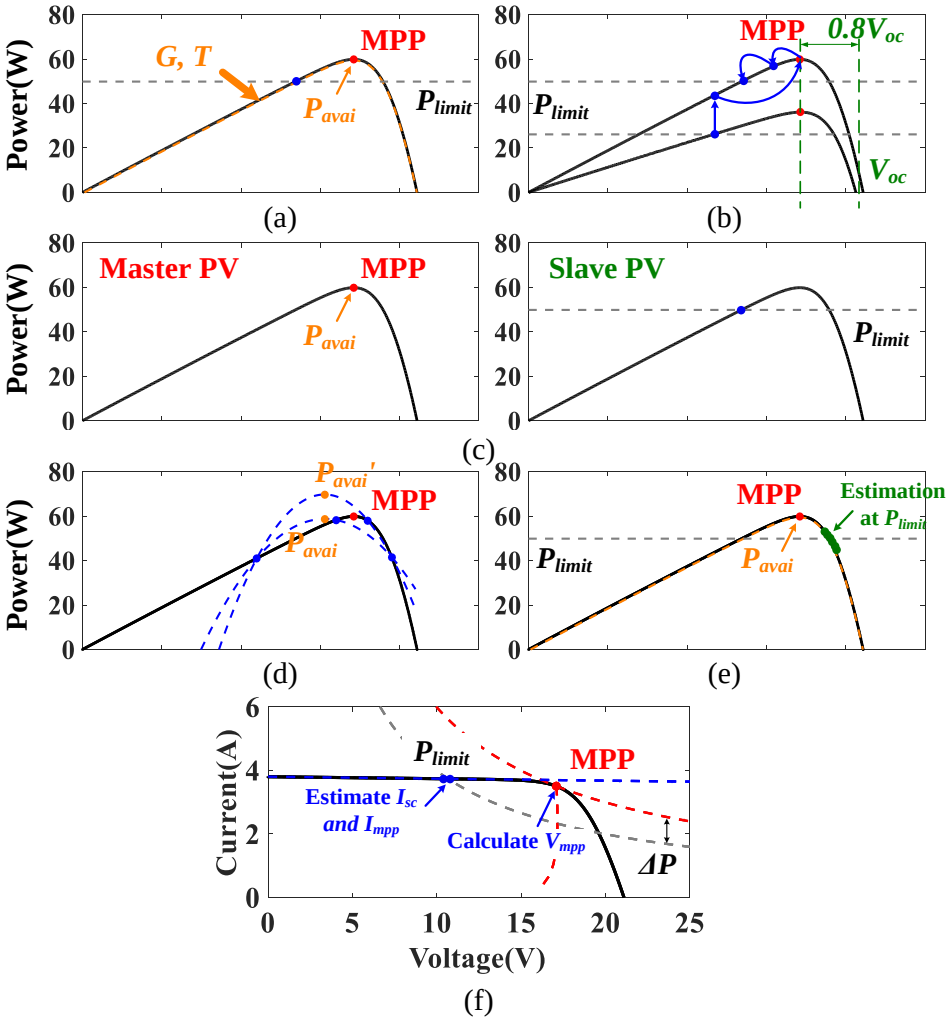

Fig. 2. Principle diagram of the P_{avai} estimation methods for the PRC: (a) by using solar irradiance and temperature sensors [30, 31], (b) by periodically entering MPPT mode [32], (c) by using a coordinate control strategy [33], (d) by using the NQI method [34], and (e) by using the WLS method [35], (f) by proposed method.

be identical rated power and geographically located close to each other with communication systems.

The second methods generally use curve fitting to estimate P_{avai}. With serval sampled operating voltage and current points, the whole P-V curve can be fitted and P_{avai} can be estimated. In [34], the P-V curve is approximately fitted to a parabolic curve with three sampled points by the Newton quadratic interpolation (NQI) method [36–38]. Accordingly, the peak of this fitted parabolic curve is considered as P_{avai}. Although the effectiveness of the NQI method has been validated in [34], the accuracy of estimated P_{avai} may be affected by the selection of the three sampled points [39]. As shown in Fig. 2 (d), the

different sampled points could result in different parabolic curves. As a consequence, the estimated P_{avai} is also varying and the accuracy of P_{avai} will be suffered. In [35], the least squares (LSQ) method is used for the P_{avai} estimation in real time. As shown in Fig. 2 (e), this method samples a large set of current and voltage values at the right side of the MPP. With these sampled points, not only P_{avai} can be estimated, but the whole P-V curve can be obtained. More important thing is that this method can estimate P_{avai} while the operating point is working at a reduced power level. However, the control implementation seems cumbersome since five parameters are required for the single-diode PV model in the real-time MPP estimation. Furthermore, in [34, 35], the operating point with a curtailed power level is allocated at the right-hand side of the MPP, which may result in the instability issue during the fast decreasing irradiance condition [32].

The main features of the previous PRC methods are demonstrated in Fig. 2 and summarized in TABLE I. As previously discussed, the aforementioned methods shows some limitations in terms of additional hardware requirements, implementation difficulty, and estimation speed. To address this issue, this paper proposes a novel PRC strategy with simple real-time MPP estimation. With the proposed control, two operating points at the left side of the true MPP are sampled to obtain the short-circuit current through estimation rather than the measurement by using additional hardware circuits. Then, the Lambert-W function is used to derive the MPP voltage and further the total available power P_{avai}. The proposed strategy requires no additional hardware such as the irradiance and temperature sensors, and it can be easily implemented in existing PV systems. With this strategy, cumbersome procedures of curve fitting with sophisticated operating points sampling and key parameters determination in the real-time MPP estimation by using the conventional PRC methods can be eliminated. This strategy is effective to provide the grid frequency support under various weather conditions even under fast solar irradiance changing condition. The proposed control can provide the grid frequency support through the direct converter duty cycle control. In order to validate the effectiveness of the proposed algorithm, a comparison of the proposed control with the control scheme in [32] is made through simulation and experimental tests under various scenarios. Main simulation and experimental results are presented to validated the advantages of the proposed method.

II. Proposed Power Reserve Control Method

A. Selection of the Suboptimal Point

As shown in Fig. 1, there are two possible suboptimal points to regulate the power working at P_{limit}, namely point A and B. Some of the relevant papers prefer the system working at the point B due to

TABLE I
COMPARISON BETWEEN THE PROPOSED METHOD AND THE PREVIOUS P_{avai} ESTIMATION METHODS FOR THE PRC

Ref.	How to obtain P_{avai}	Additional hardware requirement	Real-Time	P_{limit} location	Implantation	Estimation speed
[30, 31]	Measurement	Solar irradiance and temperature sensors	Yes	Left	Complex	Medium
[32]	Measurement	No	No	Left	Simple	Medium
[33]	Measurement	Identical PV systems	Yes	Left	Simple	Medium
[34]	Estimation	No	No	Right	Complex	Slow
[35]	Estimation	No	Yes	Right	Complex	Fast
Proposed	Separate Estimation	No	Yes	Left	Simple	Fast

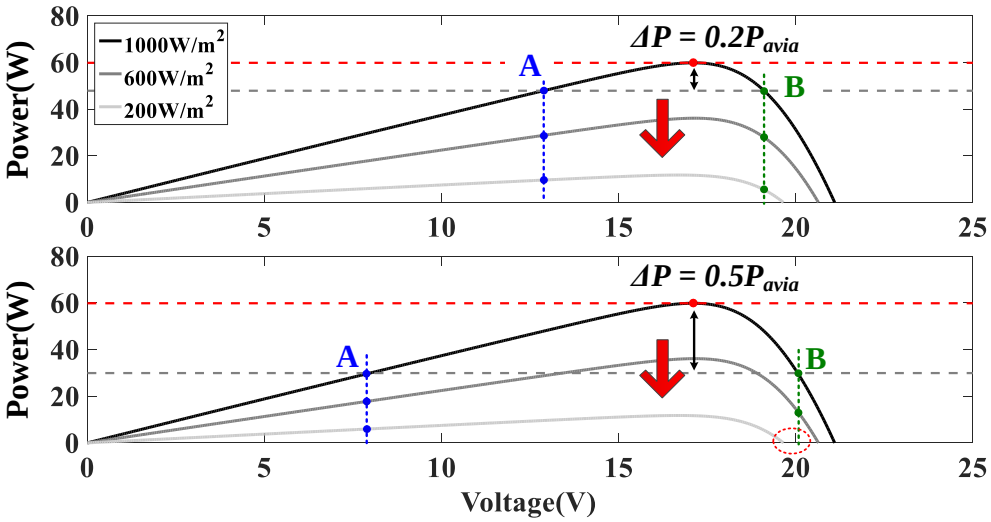

Fig. 3. Stability issue for the two suboptimal points when the solar irradiance suddenly is decreased.

higher converter efficiency and faster dynamic response [34, 35], while some of them prefer the point A due to the concern about unstable operation at the point B [30–33]. Therefore, it is very essential to select the suboptimal point.

1) Stability Issue: Fig. 3 demonstrates the stability issue when the solar irradiance is suddenly decreased. Assuming that the initial solar irradiance is 1000W/m^2 and $0.2P_{avai}$ is reserved for ΔP. When the solar irradiance is suddenly decreased to 600W/m^2 or 200W/m^2, the operating point at A and B will straightly go down along the dot lines. As shown in Fig. 3, both of the point A and B will stay at the lower solar irradiance level. However, if higher percentage of P_{avai} (e.g., 50%) is reserved for ΔP, the point B may fall into the area beyond the V_{oc} when the solar irradiance is decreased to 200W/m^2. It should be pointed out that PV systems are not allowed to immediately disconnect from the grid [33]. Under this

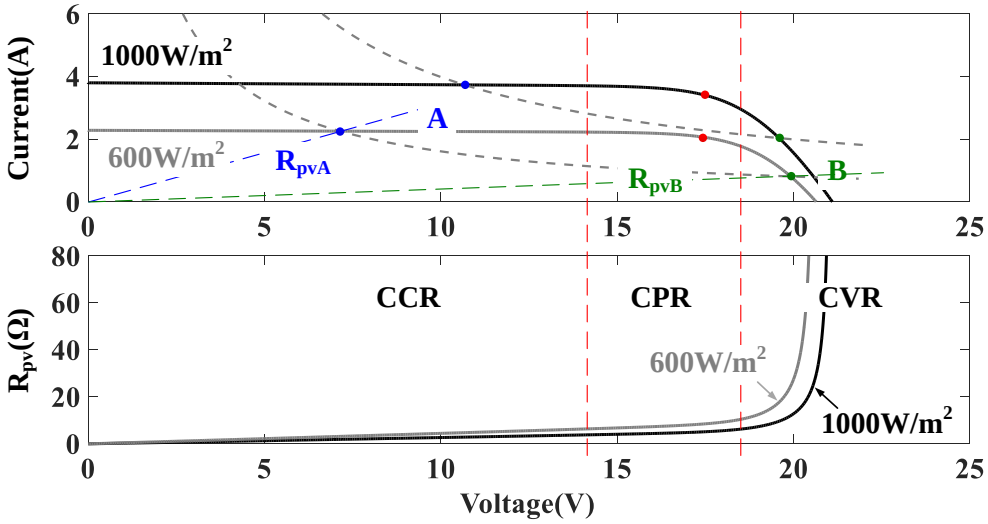

Fig. 4. Linear region of the I-V curve.

condition, the PV system is not able to produce any power to the grid, so the PRC operation becomes unstable. However, compared to the point B, whatever the solar irradiance is changed or percentage of P_{avai} is reserved, the PRC at the point A is always stable.

2) Perturbation Interval: apart from the stability issue, it is also important to choose the parameter of the perturbation interval T_p. T_p is used to ensure that the period between two successive perturbations is longer than the setting time of PV power transient [40]. Generally, T_p should be properly selected at the MPP region (or referred as the constant power region, CPR) [39]. However, when the PV system is regulated at either the point A or the point B, the system is actually working at the linear region of the I-V curve. As shown in Fig. 4, the linear regions at the point A and the point B are called as the constant current region (CCR) and the constant voltage region (CVR), respectively [41]. Therefore, the selection of T_p should be carried out considering the features of CCR or CVR if the point A or the point B is selected. According to [40], T_p in the CCR and the CVR can be derived by:

$$T_p \geq T_\varepsilon \cong -\frac{1}{\zeta \cdot \omega_n} \cdot \ln\left(\varepsilon\sqrt{1-\zeta^2}\right) \tag{2}$$

where $\omega_n = 1/\sqrt{L \cdot C_{in}}$, $\zeta = 1/(2 \cdot R_{pv}) \cdot \sqrt{L/C_{in}}$, and $\varepsilon = 0.1$.

Fig. 5 shows that PV power transients under different regions and different solar irradiance. A step change in duty cycle is used to sweep the I-V curve of the PV module. Since R_{pv} in the CCR is much smaller than that in CVR, the required setting time in the CCR is much longer than that in the CVR, as demonstrated in Fig. 5. In other words, a smaller T_p could be used in the CVR rather than the CCR.

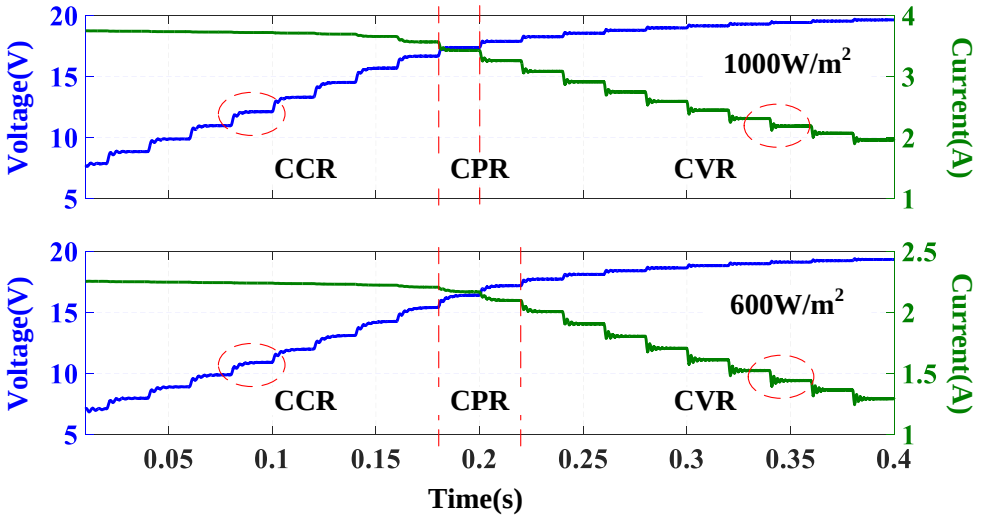

Fig. 5. PV power transient under different regions and different solar irradiance.

Therefore, the PRC at the point B could have a faster tracking speed than that at the point A.

B. Maximum Available Power Estimation

Due to the concern about the stability, the point A is selected as the suboptimal point for the PRC. As aforementioned discussion, a higher T_p has to be used to ensure the setting time is long enough to reach the steady state. A pair of voltage and current in the CCR are sampled in this algorithm to estimate P_{avai}. It is undoubted that three or more sampled points can improve the algorithm robustness against noise caused by measurement bias. However, if three or more T_p time periods are required to estimate P_{avai}, the estimation speed will be affected. As a matter of fact, the noise can be effectively reduced by setting the higher T_p [42, 43], so it is not really necessary to sample more points. Therefore, the proposed method only requires two sampled points to estimate P_{avai}. The whole process of P_{avai} estimation is demonstrated in Fig. 6.

From Fig. 6, the CCR can be expressed in a linear formula. Assuming two any points in the current-source region is known, the slope of the linear formula can be expressed as

$$m = \frac{I(k) - I(k-1)}{V(k) - V(k-1)} \tag{3}$$

where m refers to the slope of the current-source region; $I(k)$ and $V(k)$ refer to the present value of sampled current and voltage, respectively; and $I(k-1)$ and $V(k-1)$ refer to the previous value of

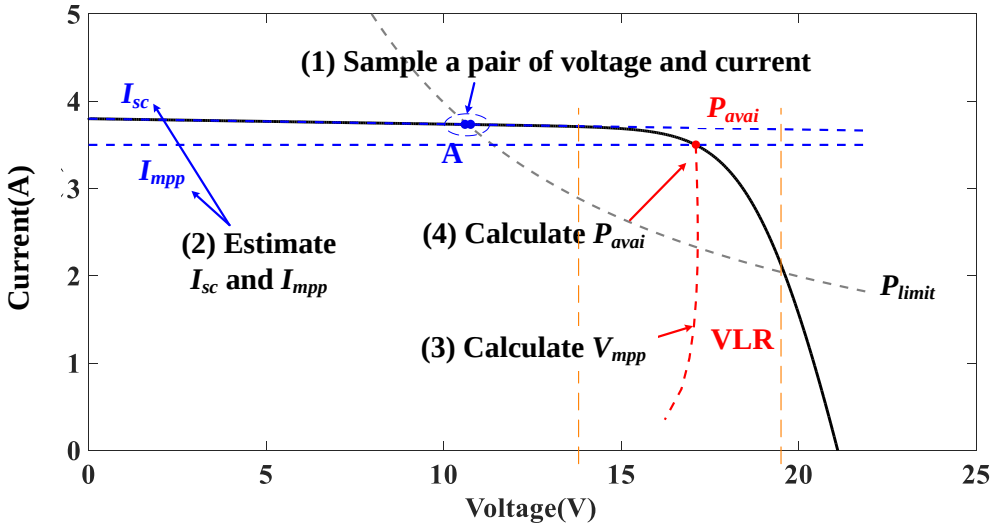

Fig. 6. Process of P_{avai} estimation.

sampled current and voltage, respectively. Then, the intercept of this linear formula, namely short-circuit current (I_{sc}) can be also obtained:

$$I_{sc} = I(k) - mV(k) \tag{4}$$

Since current at the MPP (I_{mpp}) has a near linear relationship with I_{sc}, I_{mpp} can be expressed as:

$$I_{mpp} = K_{I_{sc}} I_{sc}, 0.78 < K_{I_{sc}} < 0.92 \tag{5}$$

where $K_{I_{sc}}$ is constant [44].

Furthermore, it can be also seen that the MPP locations for different solar irradiance levels approximately lie on a straight line called as voltage linear reference (VLR) [45], marked as a red dash line in Fig.6. Therefore, V_{mpp} can be approximately expressed as a linear relationship function [45] or a nonlinear relationship function by using Lambert-W function [46]. In this paper, Lambert-W function is used to obtain V_{mpp}, namely:

$$V_{mpp} \cong \eta W \left\{ \frac{I_{mpp}\left(1 + \frac{R_s + \sqrt{R_p R_s + R_s^2}}{R_p}\right)}{I_s} \right\} - R_s I_{mpp} \tag{6}$$

where I_s is reverse saturation current, R_s and R_p are equivalent series and shunt resistances, respectively; $\eta = (N_s AKT)/q$, q is the electron charge $1.602 \times 10^{-19} C$, A is the diode ideality factor, K is Boltzmann constant $1.38 \times 10^{-23} J/K$, T(in Kelvin) is the temperature of the p–n junction, and N_s is number of series-connected cells.

TABLE II

PARAMETERS FOR THE MSX-60W PV MODULE

Parameter	Value
Maximum power P_{mpp}	$59.85W$
Voltage at MPP V_{mpp}	$17.1V$
Current at MPP I_{mpp}	$3.5A$
Open-circuit voltage V_{oc}	$21.1V$
Short-circuit current I_{sc}	$3.8A$
Temperature coefficient of V_{oc}	$-80mV/^{\circ}C$
Temperature coefficient of I_{sc}	$0.065\%/^{\circ}C$

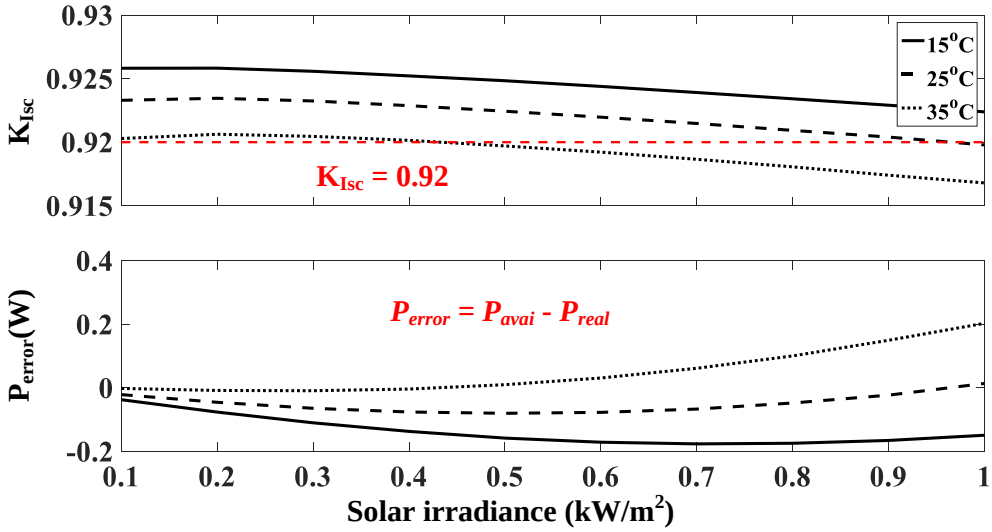

Fig. 7. $K_{I_{sc}}$ and P_{error} under different solar irradiance and temperature.

After I_{mpp} and V_{mpp} are obtained, P_{avai} can be estimated as

$$P_{avai} = P_{mpp} = V_{mpp} I_{mpp} \tag{7}$$

In order to accurately estimate P_{avai}, $K_{I_{sc}}$ is a critical parameter. In this paper, the MSX-60W PV module is used as the PV source, where its electrical specifications are shown in TABLE II. The values of $K_{I_{sc}}$ under different solar irradiance and temperature are given in Fig. 7. If $K_{I_{sc}}$ is set as 0.92, P_{avai} can be calculated by the equations (3)-(7). Then, the difference between calculated P_{avai} and the real maximum power P_{real} is defined as P_{error}. From Fig. 7, the absolute value of P_{error} is only around 0.2W, which can be negligible.

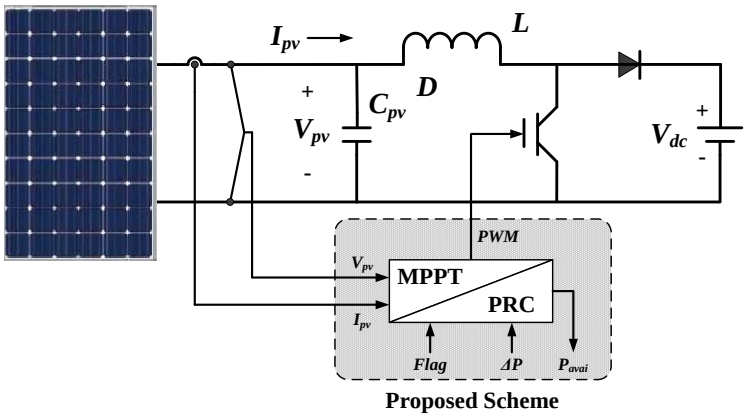

Fig. 8. Simplified PV system with a boost converter with the proposed control scheme.

C. Proposed control scheme

In [32, 33], a two-stage grid-connected PV inverter is used to validate the PRC method that they proposed. It consists of two power converters, namely a PV-side DC-DC converter and a grid-side DC-AC inverter. Generally, the PV-side DC-DC converter is responsible to regulate the PV power working at P_{mpp} or P_{limit} and the grid-side DC-AC inverter is used to deliver the extracted PV power to the AC grid. Since the DC and AC power are decoupled in the two-stage configuration, the PV-side control and the grid-side control are also decoupled. Thus, a simplified PV system with a boost converter and a resistive load is used to validate the PRC method proposed in [35]. In this paper, the boost converter with a DC load is used for simplicity, as shown in Fig. 8.

As shown in Fig. 8, the proposed control scheme consists of two working modes, namely the MPPT and the PRC. The proposed control scheme samples V_{pv} and I_{pv} from the PV side and produces PWM to realise the MPPT or the PRC. $Flag$ and ΔP are two external signals provided by the system operator, which are feeded to the proposed control scheme. $Flag$ is used to switch the working modes between the MPPT and the PRC, and ΔP is set as the required amount of reserved power. Whichever the working mode is the MPPT or the PRC, P_{avai} will be sent to the system operator and the system operator can decide $Flag$ and ΔP.

Fig. 9 shows the flowchart of the proposed control scheme. Initially, V_{pv} and I_{pv} are continually sampled, and then, $Flag$ and ΔP are provided by the system operator. If $Flag$ is equal to zero, the working mode will switch to the MPPT mode, marked as block 1 in Fig. 9. Then, a MPPT method, such as perturb and observe (P&O) method, is used to track the MPP, and the present value of sampled

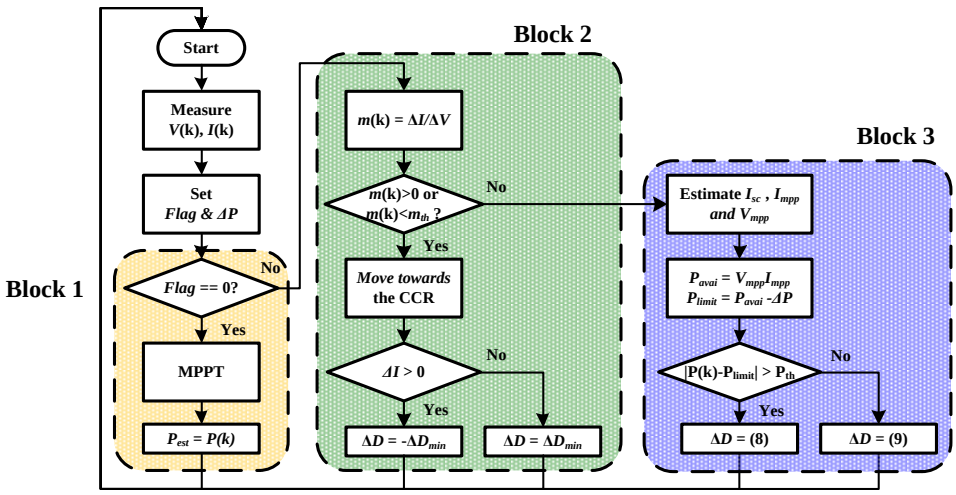

Fig. 9. Flowchart of the proposed control scheme.

power, $P(k)$, is set as P_{avai} in the steady-state stage. If $Flag$ is not equal to zero, the working mode will switch to the PRC mode, as marked a block 3 in Fig. 9. Then, I_{sc}, I_{mpp}, V_{mpp}, P_{avai} and P_{limit} can be determined in turn.

If the operating point is too far away from P_{limit}, a large step size should be used:

$$\Delta D = \begin{cases} \Delta D_{max}, \ P(k) - P_{limit} > P_{th} & \text{(8a)} \\ -\Delta D_{max}, \ P(k) - P_{limit} < -P_{th} & \text{(8b)} \end{cases}$$

ΔD refers to step size, ΔD_{max} refers to the maximum step size and P_{th} is defined as a threshold. Otherwise, the proposed algorithm will perturb around P_{limit} with a small step size.

$$\Delta D = \begin{cases} \Delta D_{min}, \ P(k) > P_{limit} & \text{(9a)} \\ -\Delta D_{min}, \ P(k) < P_{limit} & \text{(9b)} \end{cases}$$

where ΔD_{min} refers to the minimal step size.

As aforementioned discussion, P_{avai} can be estimated as long as the operating point at the CCR. Fig. 10 shows that the values of $\Delta I/\Delta V$ around P_{limit} are approximately equal to zero even though the solar irradiance is different. Therefore, $\Delta I/\Delta V$ can be used as an index, which determine whether the operating point is at the CCR Then, it can be expressed as:

$$m_{th} < m(k) = \frac{\Delta I}{\Delta V} = \frac{I(k) - I(k-1)}{V(k) - V(k-1)} < 0 \tag{10}$$

where $m(k)$ refers to the present value of $\Delta I/\Delta V$. Since the value of $\Delta I/\Delta V$ around P_{limit} is not exactly equal to zero at the CCR, a threshold, m_{th}, and a boundary are defined in (10). As marked in a

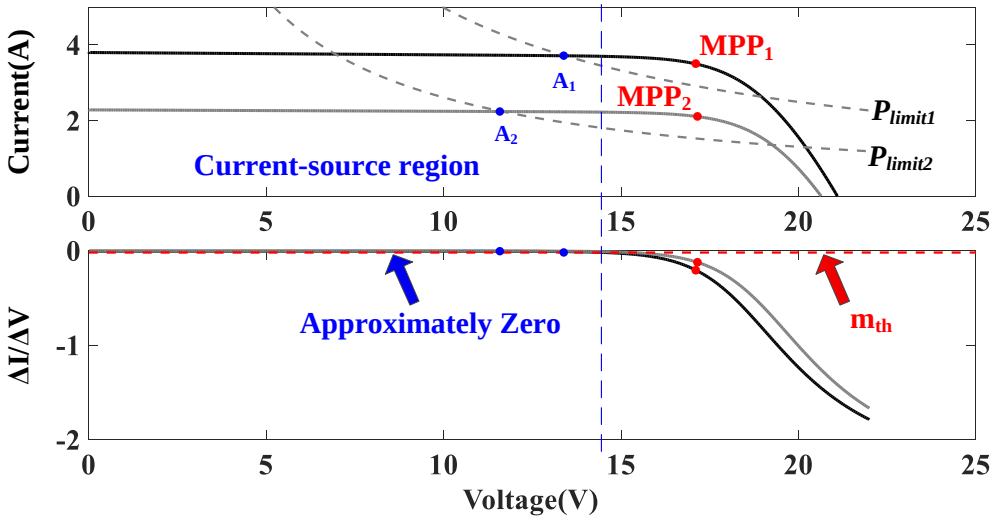

Fig. 10. I-V and ΔI-ΔV curve.

block 2 in Fig. 9, if the value of $m(k)$ is within this boundary, the algorithm will go through the block 3. Otherwise, the algorithm will go through the block 2 and move towards the CCR.

D. Grid Frequency Support Scheme

From Fig. 8, three signal ports, $Flag$, ΔP and P_{avai}, are encapsulated. The three encapsulated signal ports can be directly controlled by system operator. Therefore, how to use these signals to support the grid frequency responses will be demonstrated in this subsection.

Fig. 11 demonstrates how the proposed method supports the grid frequency response. Based on the changes of ΔP and ΔG, there are three possibilities:

1) Only ΔP changes: Assume that the solar irradiance is maintained unchanged. When a major contingency happens, such as a sudden reduction of the generator output power, the reserved power should be provided to response the grid frequency. Then, ΔP will be decreased by the system operator, as shown in Fig. 11 (a). If all of the reserved power have to immediately feed to the grid, $Flag$ in the flowchart Fig. 9 will be set as "0" and the operation mode will be changed to the MPPT mode by the system operator. Then, some fast MPPT methods, such as Beta method [47], can make the operating point immediately move the MPP within several seconds. After the grid frequency is restored back, $Flag$ is set as "1" according to the flowchart shown in Fig. 9 and the operation mode is changed to the PRC mode in order to restore ΔP again, as shown in Fig. 11 (b).

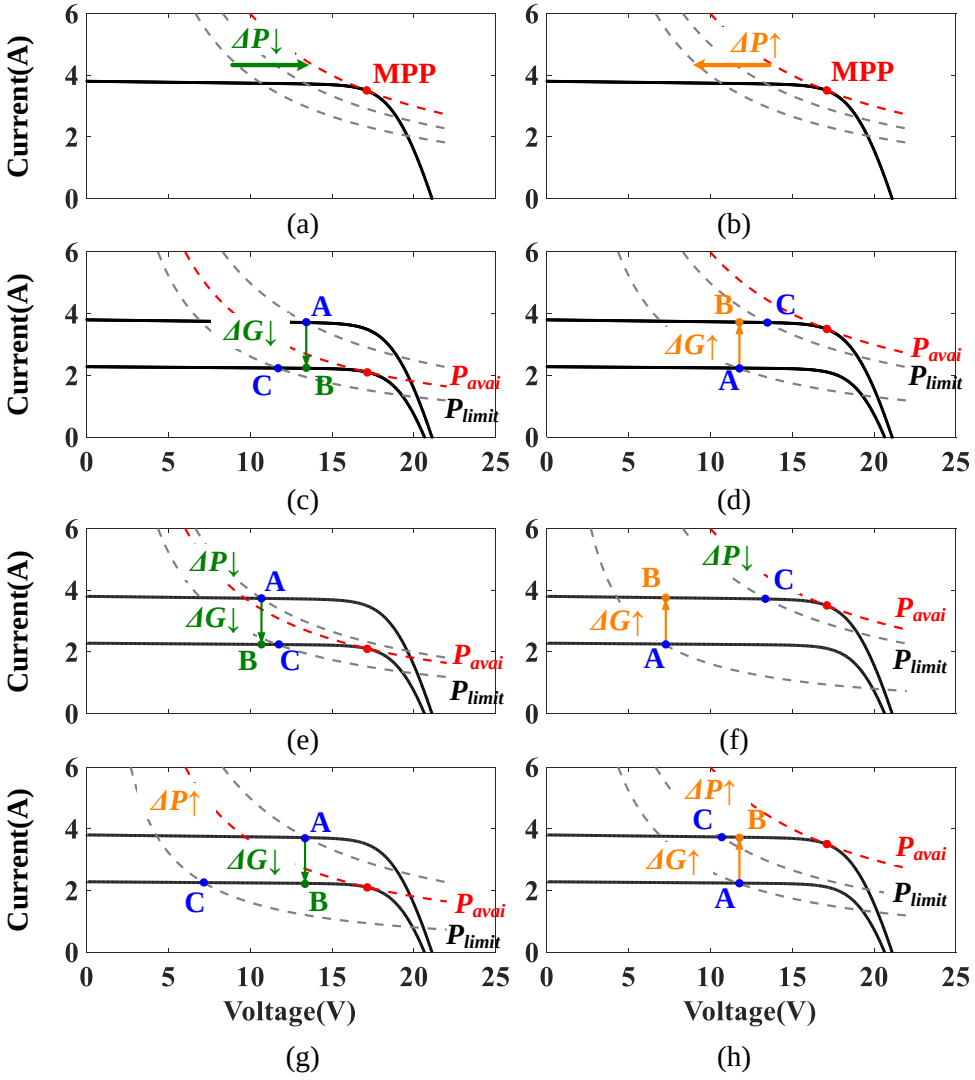

Fig. 11. Demonstration of grid frequency support scheme by the proposed method. (a) ΔP decreases; (b) ΔP increases; (c) ΔG decreases; (d) ΔG increases; (e) ΔP and ΔG decrease; (f) ΔP decreases and ΔG increases; (g) ΔP increases and ΔG decreases; (h) ΔP and ΔG increase.

It should be noted that the operating point is actually working at the PRC under this situation. The measured $m(k)$ is always satisfied with the equation (10), and the proposed method only goes through the block 3 in Fig. 9.

2) Only ΔG changes: Assume that ΔP is maintained unchanged. When the solar irradiance is changed, it is essential to maintain the reserved power ΔP always at a certain value during this period. Fig. 11 (c) and (d) demonstrates the changes of solar irradiance ΔG. Assuming that point A is the initial point

before the change of ΔG happened and point C is the optimal point after the change of ΔG happened. Whatever ΔG decreases or increases, the operating point will directly go down or go up from A to B. At this time, since point B is already in the CCR, the proposed method just slightly perturbs the operating point as shown in the block 2 in Fig. 9. The perturbation in the converter duty cycle is expressed as:

$$\Delta D = \begin{cases} \Delta D_{min},\ \Delta I < 0 & \text{(11a)} \\ -\Delta D_{min},\ \Delta I > 0 & \text{(11b)} \end{cases}$$

3) Both of ΔP and ΔG will change: Fig. 11 (e)-(h) demonstrates the case with both the changes in ΔP and ΔG. Point A and C refer to the initial point and the optimal point, respectively. Whatever ΔP and ΔG decrease or increase, the operating point will directly go down or go up from A to B. From Fig. 11 (e)-(h), whatever the changes in ΔP and ΔG are positive or negative, B is very close to C. Therefore, the proposed method just slightly perturbs the operating point with a small step size change obtained with the equation (9). Otherwise, considering that B is far away from C, a large step size change obtained from the equation (8) is used.

III. Simulation

In order to prove the effectiveness of the proposed control scheme, a boost converter is used, as shown in Fig. 8. The input capacitor, output capacitor, inductor and switching frequency for the boost converter are $470uF$, $47uF$, $1mH$ and $20kHz$, respectively. The output DC voltage is 24V. D_{min} and D_{max} are set as 0.5 and 2, respectively. $K_{I_{sc}}$ is set as 0.92 and m_{th} is set as -0.02. The perturbation time for the proposed method, T_p, is $0.03s$.

A. Reserved Power Command Change

Fig. 12 shows that simulation results for the proposed control scheme when ΔP is changed. P_{pv}, V_{pv} and I_{pv} refer to the PV output power, voltage and current, respectively. P_{avai} refers to the maximum available power estimated by the proposed control scheme and P_{ideal} refers to the ideal maximum power. ΔP refers to the power reserved by the proposed control scheme and ΔP_{ideal} refers to the power which should be reserved by the system.

Initially, the PV system works at the MPPT mode. At time 0.5s, the PRC is activated and ΔP is set as 10W. After that, ΔP is changed in every 0.5s varying among 10W, 15W and 20W. Finally, the MPPT mode is activated at time 3s. During the whole simulation time, the solar irradiance maintains at 1000W/m^2.

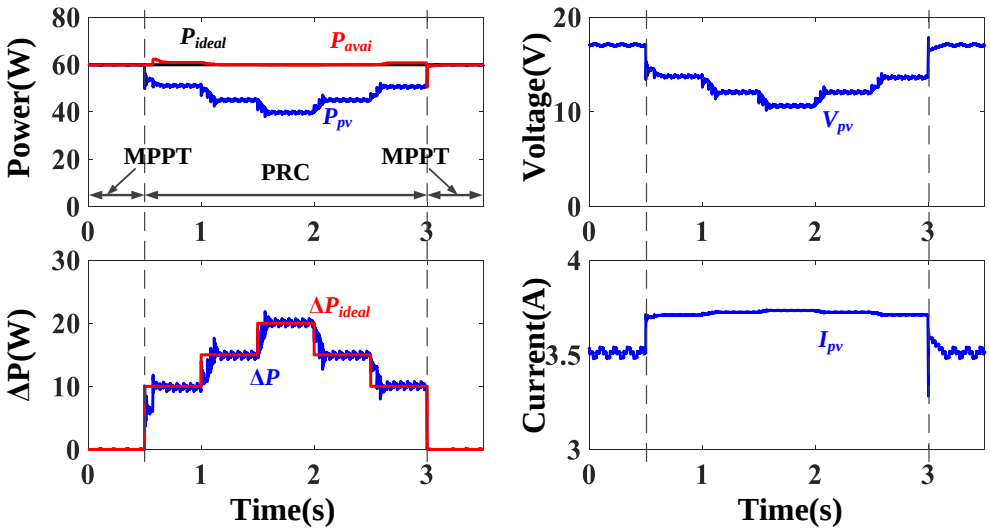

Fig. 12. Simulation results for the proposed control scheme when ΔP is changed.

As shown in Fig. 12, the proposed control scheme successfully tracks with the step changes of ΔP. The actual reserved power ΔP is just fitted to the profile of ΔP_{ideal}. Since the operating point is already in the CCR, P_{avai} can be directly obtained. To be more specific, it requires averagely 2 to 3 steps to response the step changes of ΔP. Therefore, the tracking speed is also very fast.

B. Solar Irradiance Change

Fig. 13 shows that simulation results for the proposed control scheme when ΔG is changed. ΔP is fixed at 10W during the whole simulation time, while the PRC mode is activated during the time 0.5s to 5s. The solar irradiance maintains at 600W/m^2 from 0s to 1s, and increases by 100W/m^2 in every 0.5s until it reaches 1000W/m^2. Then, the solar irradiance decreases by 100W/m^2 in every 0.5s until 600W/m^2. Finally, the solar irradiance maintains at 600W/m^2 again, from 4.5s to 5.5s.

As shown in Fig. 13, the proposed control scheme also successfully tracks when ΔG is changed. The proposed control scheme only needs 2 or 3 steps to reach the new P_{limit} when the solar irradiance changes. ΔP is just fitted to the profile of ΔP_{ideal} and ΔP almost maintains at 10W during the PRC mode.

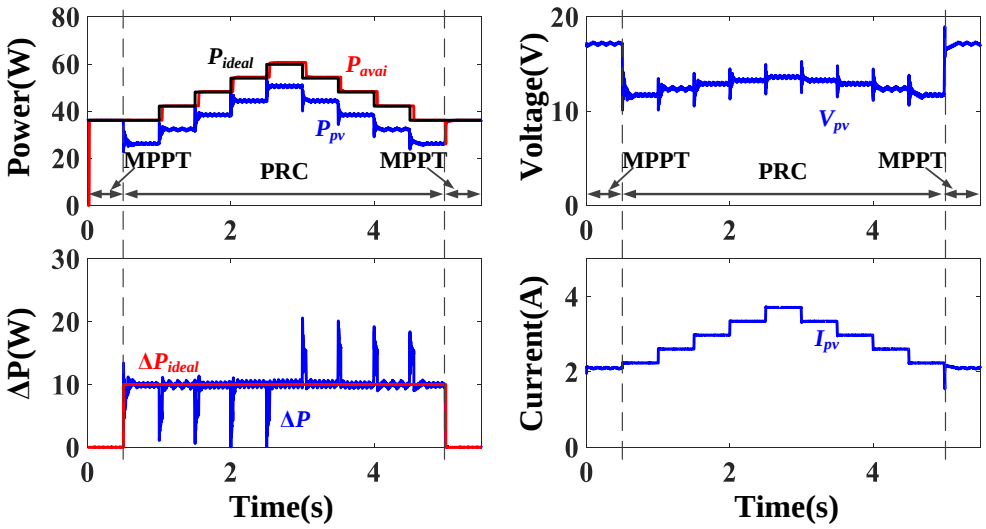

Fig. 13. Simulation results for the proposed control scheme when ΔG is changed.

C. Both of Reserved Power Command and Solar Irradiance Change

Fig.13 shows that simulation results for the proposed control scheme when ΔP and ΔG are changed. The PRC mode is activated during the time 0.5s to 3s. The initial solar irradiance and ΔP are 1000W/m^2 and 20W, respectively. At time 1s, 1.5s, 2s and 2.5s, both of the solar irradiance and ΔP are changed as following trajectory:

- 1000W/m^2 $\rightarrow$ 900W/m^2 $\rightarrow$ 1000W/m^2 $\rightarrow$ 900W/m^2 $\rightarrow$ 1000W/m^2
- 20W $\rightarrow$ 15W $\rightarrow$ 10W $\rightarrow$ 15W $\rightarrow$ 20W

As shown in Fig. 13, the proposed control scheme also successfully tracks when ΔP and ΔG are changed. The proposed control scheme also needs 2 or 3 steps to reach the new P_{limit} and ΔP is just fitted to the profile of ΔP_{ideal}.

D. Comparison with the Other PRC Method

In order to highlight the advantages of the proposed method, the control scheme in [32] is used to make a comparison. Based on the operational principle in [32], the control scheme in [32] is well optimized. Same simulation setup as the proposed is used, the simulation results for the control scheme in [32] are shown in Fig. 15.

As description in [32], the fractional open-circuit voltage MPPT method is periodically used to measure P_{avai} rather to estimate it. As shown in Fig. 15, the operating point directly moves to the position of $0.8V_{oc}$

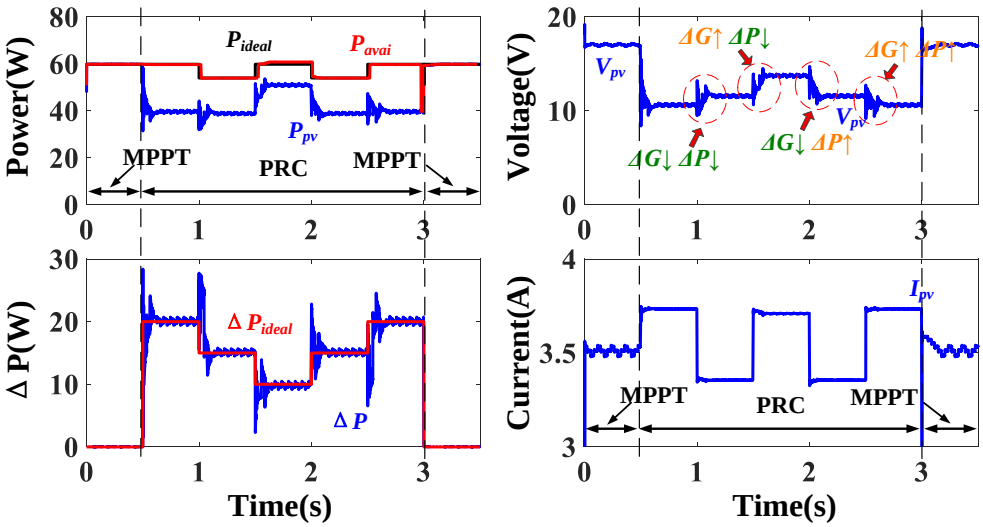

Fig. 14. Simulation results for the proposed control scheme when ΔP and ΔG are changed.

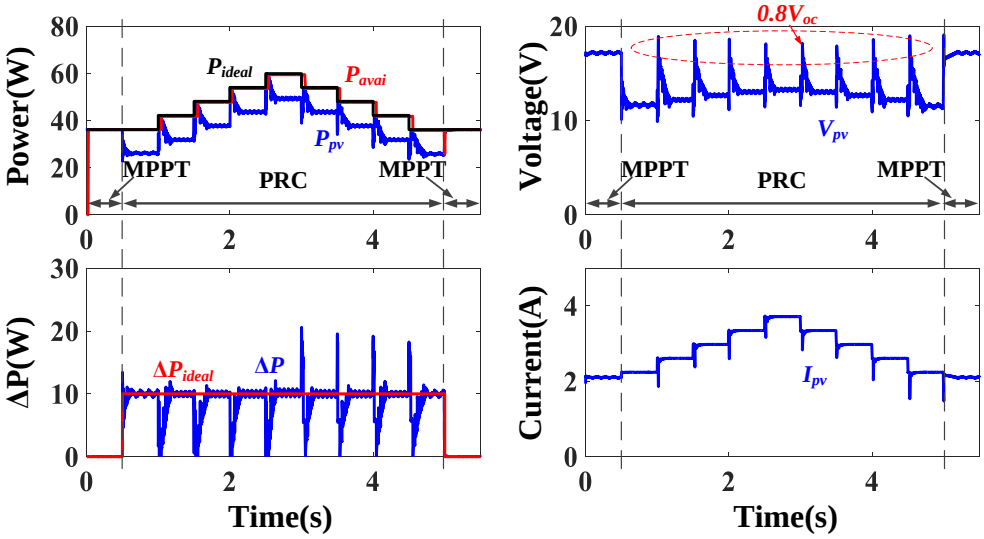

Fig. 15. Simulation results for the control scheme in [32] when the solar irradiance is changed.

when the solar irradiance changes. Once P_{avai} is measured, the operating point is gradually perturbed to P_{limit}. Power and voltage ripples during the changes of the solar irradiance can be clearly seen from Fig. 15.

In order to compare the performance of the proposed method and the control scheme in [32], the

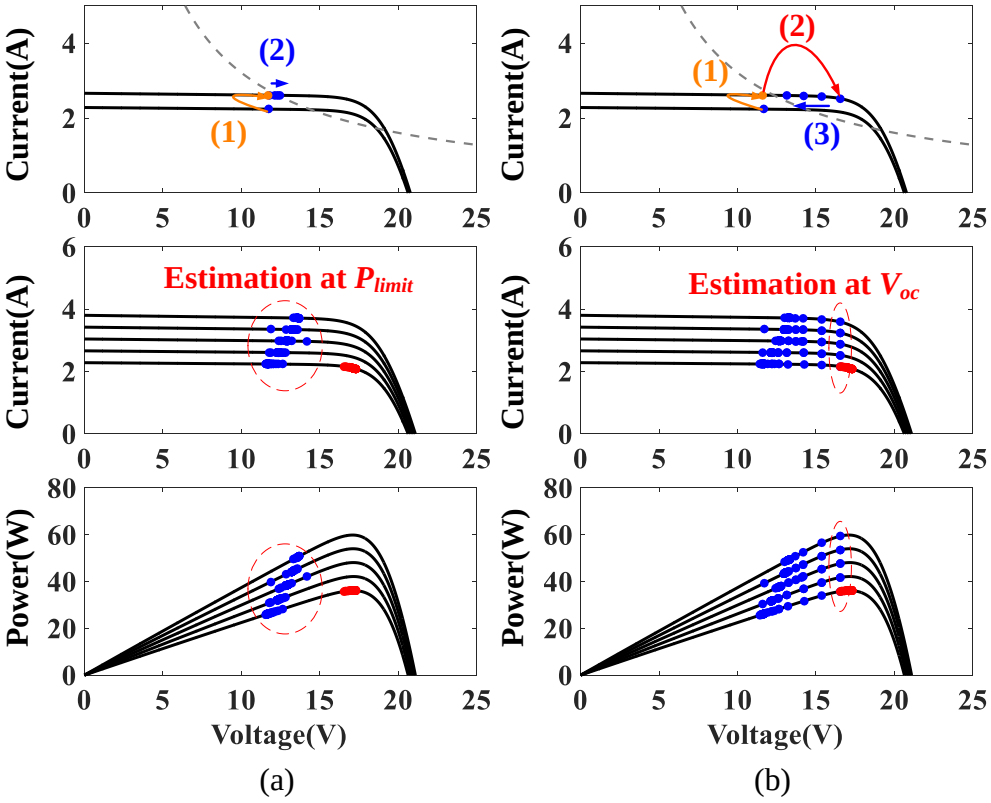

Fig. 16. Movements of the operating points and operating trajectory when the solar irradiance is increased. (a) Proposed method; (b) Method in [32].

movements of the operating points and the corresponding operating trajectories by using these two methods are demonstrated in Fig. 16. Fig. 16 (a) illustrates the movements of the operating points by using the proposed method when the solar irradiance is increased. It can be seen that the operating point straightly goes up, marked as (1) in Fig. 16 (a). Since the operating point is already in the CCR, P_{avai} can be estimated at the optimal P_{limit}, marked as (2) in Fig. 16 (a). Compared to the proposed method, the control scheme in [32] has to move the position of $0.8V_{oc}$ to measure P_{avai} rather to estimate it. As a consequence, one more step as marked red text (2) in Fig. 16 (b) is needed. Furthermore, the movement to $0.8V_{oc}$ also causes several extra steps back to P_{limit}.

The operating trajectories by using the proposed method and the control scheme in [32] are also demonstrated in Fig. 16, where the red dots refer to the operating trajectory for the MPPT mode while the blue dots refer to that for the PRC mode. Unlike the control scheme in [32], the proposed control scheme only needs to work around the CCR to estimate P_{avai}. It is not necessary to sample the points

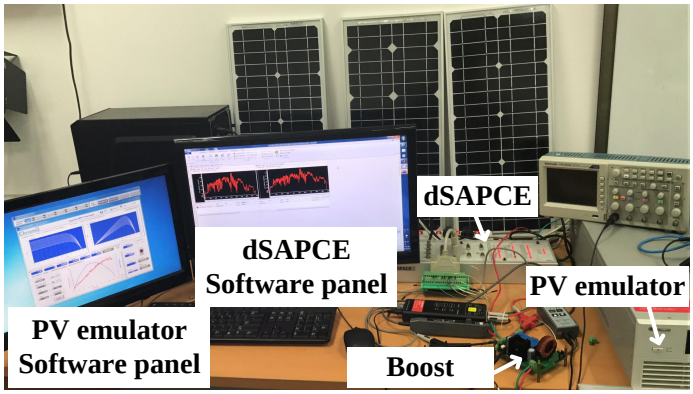

Fig. 17. Experimental setup of the simplified PV system with a boost converter.

around the MPP region. That is the reason why the proposed control will be regulated always operating at P_{limit}.

IV. Experimental results

In order to verify the effectiveness of the proposed PRC method, the experimental tests are carried out with the experimental prototypes shown in Fig. 17. Main specification of the main components are identical to the simulation. The PV emulator Chroma ATE-62050H-600S, which is a programmable DC supply, is used to emulate solar module characteristics. The dSPACE DS1104 is adopted as a control platform where the proposed PRC method is implemented in it. The electronic load, IT8514C+, is used and it works at the constant voltage (CV) mode The sampling time T_p for the proposed method in the experiments was set as $0.1s$.

Fig. 18 shows that experimental results for the proposed control scheme. First, a constant solar irradiance profile of $1000W/m^2$ is used to be evaluated. Three values of ΔP, namely 10W, 15W and 20W, are used to verify the effectiveness of the proposed method when ΔP changes. As shown in Fig. 18 (a), the proposed control scheme successfully tracks with the step changes of ΔP. The actual reserved power ΔP is just fitted to the profile of ΔP_{ideal}.

Furthermore, the proposed method is also verified when the solar irradiance changes. Similar to the simulation, ΔP is fixed at 10W during the whole experiment time and the solar irradiance varies from $600W/m^2$ to $1000W/m^2$. As shown in Fig. 18 (b), the proposed control scheme also successfully tracks with the solar irradiance changes. The proposed control scheme only needs several steps to reach the new P_{limit} when the solar irradiance changes. ΔP is just fitted to the profile of ΔP_{ideal} and ΔP almost maintains at 10W during the PRC mode.

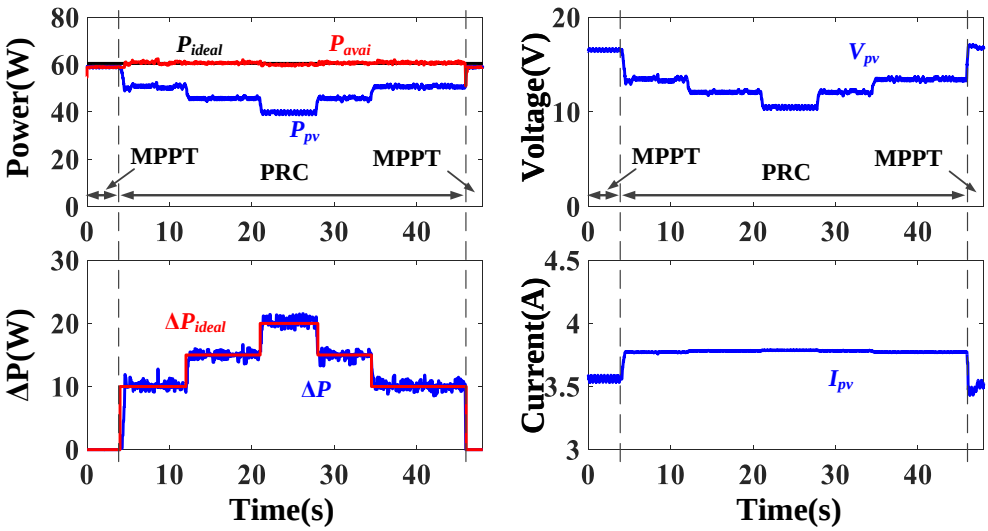

(a)

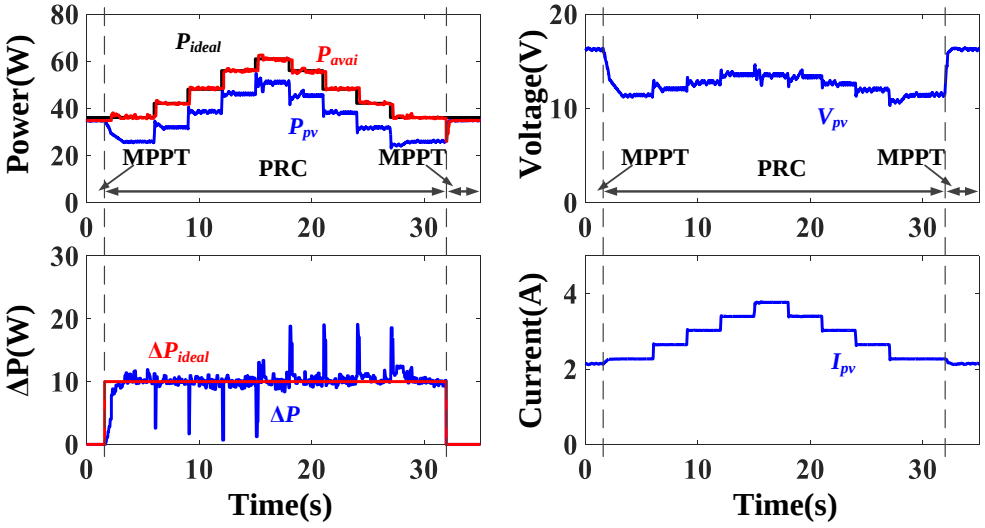

(b)

Fig. 18. Experimental results for the proposed control scheme. (a) ΔP is changed; (b) Solar irradiance is changed.

In order to further verify the effectiveness of the proposed method in real life, the real-field meteorological data are programmed in the PV emulator. The meteorological data of two distinct locations, namely University of Nevada, Las Vegas (UNLV) and Humboldt State University (HSU), California, are selected as shown in Fig. 19 (a) and Fig. 20 (a), respectively. It is noticeable that meteorological profiles in UNLV and HSU refer to a clear day and a cloudy day, respectively. Besides, the solar irradiation could

vary dramatically in a daily day, however, the temperature just changes slightly.

It should be also noted that the original irradiance data is at 1 min resolution, which takes 7 to 8 hours to carry out the one experiment for one days data. In order to save the experimental time, the resolution of irradiance data has been updated as 2 seconds. Furthermore, a period of time (i.e, from 7:49:00 to 15:43:00 in UNLV and from 8:13:00 to 16:03:00 in HSU) is adopted to accelerate the experiment.

Fig. 19 (b) shows that the PRC mode with 10W reserved power is used in a clear day. It can be seen clearly that ΔP is just fitted to the profile of ΔP_{ideal} and the power reserve can be accurately controlled at 10W during the whole process. Besides, another test with the operational mode transition (i.e., MPPT$\rightarrow$PRC$\rightarrow$MPPT) is also verified in this clear day. As shown in Fig. 19 (c), it should be noted that the response time between the MPPT mode and the PRC mode is also very quick and the power reserve can be accurately controlled at 10W during the PRC mode.

Fig.20 (b) and (c) show that the PRC mode with 10W and 20W reserved power and the operational mode transition is used in a cloudy day, respectively. It can be seen that the proposed method is also very effective under fast solar irradiance changing as well as operational mode changes. As a conclusion, these experimental results verify effectiveness of the proposed method under various weather conditions.

V. Conclusion

In this paper, a novel PRC method is proposed with a boost converter. A comparison between the proposed method and the previous P_{avai} estimation methods for the PRC is shown in TABLE I. Compared to the prior PRC methods, four main advantages of the proposed method can be summarised:

1) The proposed method can be implemented without any additional hardware requirements.
2) Unlike the other methods, P_{avai} is estimated separately in separate steps rather than directly estimated or measured.
3) Furthermore, the proposed method can always to operate at P_{limit}.
4) Besides, the proposed method is very fast and effective under various weather conditions, especially under fast solar irradiance changing.

Both of simulation and experimental results validated the effectiveness of the proposed method. Various testing conditions between the proposed method and the control scheme in [32] are compared and analyzed. The proposed method is encapsulated with three signal ports, which can be directly controlled by system operator and provided to support the grid frequency responses.

REFERENCES

[1] S. Kouro, J. I. Leon, D. Vinnikov, and L. G. Franquelo, "Grid-connected photovoltaic systems: An overview of recent research and emerging pv converter technology," *IEEE Ind. Electron. Mag.*, vol. 9, no. 1, pp. 47–61, Mar. 2015.

[2] Y. Liu, S. You, J. Tan, Y. Zhang, and Y. Liu, "Frequency response assessment and enhancement of the u.s. power grids toward extra-high photovoltaic generation penetrations-an industry perspective," *IEEE Trans. Power Syst.*, vol. 33, no. 3, pp. 3438–3449, May 2018.

[3] S. Eftekharnejad, V. Vittal, G. T. Heydt, B. Keel, and J. Loehr, "Impact of increased penetration of photovoltaic generation on power systems," *IEEE Trans. Power Syst.*, vol. 28, no. 2, pp. 893–901, May 2013.

[4] ——, "Small signal stability assessment of power systems with increased penetration of photovoltaic generation: A case study," *IEEE Trans. Sustain. Energy*, vol. 4, no. 4, pp. 960–967, Oct. 2013.

[5] B. Tamimi, C. Caizares, and K. Bhattacharya, "System stability impact of large-scale and distributed solar photovoltaic generation: The case of ontario, canada," *IEEE Trans. Sustain. Energy*, vol. 4, no. 3, pp. 680–688, Jul. 2013.

[6] M. Dreidy, H. Mokhlis, and S. Mekhilef, "Inertia response and frequency control techniques for renewable energy sources: A review," *Renew. Sust. Energ. Rev.*, vol. 69, pp. 144–155, 2017.

[7] Y. Bae, T.-K. Vu, and R.-Y. Kim, "Implemental control strategy for grid stabilization of grid-connected pv system based on german grid code in symmetrical low-to-medium voltage network," *IEEE Trans. Energy Convers.*, vol. 28, no. 3, pp. 619–631, Sep. 2013.

[8] W. A. Omran, M. Kazerani, and M. M. A. Salama, "Investigation of methods for reduction of power fluctuations generated from large grid-connected photovoltaic systems," *IEEE Trans. Energy Conver.*, vol. 26, no. 1, pp. 318–327, Mar. 2011.

[9] G. Delille, B. Francois, and G. Malarange, "Dynamic frequency control support by energy storage to reduce the impact of wind and solar generation on isolated power system's inertia," *IEEE Trans. Sustain. Energy*, vol. 3, no. 4, pp. 931–939, Oct. 2012.

[10] S. Chen, T. Zhang, H. B. Gooi, R. D. Masiello, and W. Katzenstein, "Penetration rate and effectiveness studies of aggregated bess for frequency regulation," *IEEE Trans. Smart Grid*, vol. 7, no. 1, pp. 167–177, Jan. 2016.

[11] J. C. Hernndez, P. G. Bueno, and F. Sanchez-Sutil, "Enhanced utility-scale photovoltaic units with frequency support functions and dynamic grid support for transmission systems," *IET Renew. Power Gen.*, vol. 11, no. 3, pp. 361–372, 2017.

[12] P. C. Sekhar and S. Mishra, "Storage free smart energy management for frequency control in a diesel-pv-fuel cell-based hybrid ac microgrid," *IEEE Trans. Neur. Net. Lear. Syst.*, vol. 27, no. 8, pp. 1657–1671, Aug. 2016.

[13] B. I. Craciun, T. Kerekes, D. Sera, and R. Teodorescu, "Frequency support functions in large pv power plants with active power reserves," *IEEE J. Em. Sel. Top. P.*, vol. 2, no. 4, pp. 849–858, Dec. 2014.

[14] C. Rahmann and A. Castillo, "Fast frequency response capability of photovoltaic power plants: The necessity

of new grid requirements and definitions," *Energies*, vol. 7, no. 10, pp. 6306–6322, 2014.

[15] C. Rahmann, V. Vittal, J. Ascui, and J. Haas, "Mitigation control against partial shading effects in large-scale pv power plants," *IEEE Trans. Sustain. Energy*, vol. 7, no. 1, pp. 173–180, Jan. 2016.

[16] P. Zarina, S. Mishra, and P. Sekhar, "Exploring frequency control capability of a pv system in a hybrid pv-rotating machine-without storage system," *Int. J. Elec. Power Energy Syst.*, vol. 60, pp. 258 – 267, 2014.

[17] R. Luthander, D. Lingfors, and J. Widn, "Large-scale integration of photovoltaic power in a distribution grid using power curtailment and energy storage," *Sol. Energy*, vol. 155, pp. 1319 – 1325, 2017.

[18] A. Sangwongwanich, Y. Yang, and F. Blaabjerg, "Development of flexible active power control strategies for grid-connected photovoltaic inverters by modifying mppt algorithms," in *2017 IEEE 3rd International Future Energy Electronics Conference and ECCE Asia (IFEEC 2017 - ECCE Asia)*, Jun. 2017, pp. 87–92.

[19] ——, "High-performance constant power generation in grid-connected pv systems," *IEEE Trans. Power Electron.*, vol. 31, no. 3, pp. 1822–1825, Mar. 2016.

[20] A. Sangwongwanich, Y. Yang, F. Blaabjerg, and H. Wang, "Benchmarking of constant power generation strategies for single-phase grid-connected photovoltaic systems," *IEEE Trans. Ind. Appl.*, vol. 54, no. 1, pp. 447–457, Jan. 2018.

[21] H. D. Tafti, A. I. Maswood, G. Konstantinou, J. Pou, and F. Blaabjerg, "A general constant power generation algorithm for photovoltaic systems," *IEEE Trans. Power Electron.*, vol. 33, no. 5, pp. 4088–4101, May 2018.

[22] B. Crciun, T. Kerekes, D. Sra, R. Teodorescu, and U. D. Annakkage, "Power ramp limitation capabilities of large pv power plants with active power reserves," *IEEE Trans. Sustain. Energy*, vol. 8, no. 2, pp. 573–581, Apr. 2017.

[23] Y. Karimi, H. Oraee, M. S. Golsorkhi, and J. M. Guerrero, "Decentralized method for load sharing and power management in a pv/battery hybrid source islanded microgrid," *IEEE Trans. Power Electron.*, vol. 32, no. 5, pp. 3525–3535, May 2017.

[24] Y. Karimi, H. Oraee, and J. M. Guerrero, "Decentralized method for load sharing and power management in a hybrid single/three-phase-islanded microgrid consisting of hybrid source pv/battery units," *IEEE Trans. Power Electron.*, vol. 32, no. 8, pp. 6135–6144, Aug. 2017.

[25] M. Saleh, L. Meek, M. A. S. Masoum, and M. Abshar, "Battery-less short-term smoothing of photovoltaic generation using sky camera," *IEEE Trans. Ind. Inform.*, vol. 14, no. 2, pp. 403–414, Feb. 2018.

[26] X. Chen, Y. Du, H. Wen, L. Jiang, and W. Xiao, "Forecasting based power ramp-rate control strategies for utility-scale pv systems," *IEEE Trans. Ind. Electron.*, pp. 1–1, 2018.

[27] Y. Yang, E. Koutroulis, A. Sangwongwanich, and F. Blaabjerg, "Pursuing photovoltaic cost-effectiveness: Absolute active power control offers hope in single-phase pv systems," *IEEE Ind. Appl. Mag.*, vol. 23, no. 5, pp. 40–49, Sep. 2017.

[28] Y. Yang, H. Wang, F. Blaabjerg, and T. Kerekes, "A hybrid power control concept for pv inverters with reduced thermal loading," *IEEE Trans. Power Electron.*, vol. 29, no. 12, pp. 6271–6275, Dec. 2014.

[29] E. I. Batzelis, S. Papathanassiou, and B. C. Pal, "Pv system control to provide active power reserves under partial shading conditions," *IEEE Trans. Power Electron.*, pp. 1–1, 2018.

[30] A. Hoke, E. Muljadi, and D. Maksimovic, "Real-time photovoltaic plant maximum power point estimation for use in grid frequency stabilization," in *Proc. IEEE 16th Control Model. Power Electron. (COMPEL)*, July 2015, pp. 1–7.

[31] A. F. Hoke, M. Shirazi, S. Chakraborty, E. Muljadi, and D. Maksimovic, "Rapid active power control of photovoltaic systems for grid frequency support," *IEEE J. Em. Sel. Top. P.*, vol. 5, no. 3, pp. 1154–1163, Sep. 2017.

[32] A. Sangwongwanich, Y. Yang, and F. Blaabjerg, "A sensorless power reserve control strategy for two-stage grid-connected pv systems," *IEEE Trans. Power Electron.*, vol. 32, no. 11, pp. 8559–8569, Nov. 2017.

[33] A. Sangwongwanich, Y. Yang, F. Blaabjerg, and D. Sera, "Delta power control strategy for multistring grid-connected pv inverters," *IEEE Trans. Ind. Appl.*, vol. 53, no. 4, pp. 3862–3870, Jul. 2017.

[34] H. Xin, Y. Liu, Z. Wang, D. Gan, and T. Yang, "A new frequency regulation strategy for photovoltaic systems without energy storage," *IEEE Trans. Sustain. Energy*, vol. 4, no. 4, pp. 985–993, Oct. 2013.

[35] E. I. Batzelis, G. E. Kampitsis, and S. A. Papathanassiou, "Power reserves control for pv systems with real-time mpp estimation via curve fitting," *IEEE Trans. Sustain. Energy*, vol. 8, no. 3, pp. 1269–1280, Jul. 2017.

[36] N. Femia, D. Granozio, G. Petrone, G. Spagnuolo, and M. Vitelli, "Predictive adaptive mppt perturb and observe method," *IEEE Trans. Aero. Electron. Sys.*, vol. 43, no. 3, pp. 934–950, Jul. 2007.

[37] F. S. Pai, R. M. Chao, S. H. Ko, and T. S. Lee, "Performance evaluation of parabolic prediction to maximum power point tracking for pv array," *IEEE Trans. Sustain. Energy*, vol. 2, no. 1, pp. 60–68, Jan. 2011.

[38] Y. Liu, H. Xin, Z. Wang, and T. Yang, "Power control strategy for photovoltaic system based on the newton quadratic interpolation," *IET Renew. Power Gen.*, vol. 8, no. 6, pp. 611–620, Aug. 2014.

[39] N. Femia, G. Petrone, G. Spagnuolo, and M. Vitelli, *Power Electronics and Control Techniques for Maximum Energy Harvesting in Photovoltaic Systems*. CRC Press, 2012.

[40] J. Kivimki, S. Kolesnik, M. Sitbon, T. Suntio, and A. Kuperman, "Revisited perturbation frequency design guideline for direct fixed-step maximum power point tracking algorithms," *IEEE Trans. Ind. Electron*, vol. 64, no. 6, pp. 4601–4609, Jun. 2017.

[41] W. Xiao, W. G. Dunford, P. R. Palmer, and A. Capel, "Regulation of photovoltaic voltage," *IEEE Trans. Ind. Electron.*, vol. 54, no. 3, pp. 1365–1374, Jun. 2007.

[42] H. Al-Atrash, I. Batarseh, and K. Rustom, "Effect of measurement noise and bias on hill-climbing mppt algorithms," *IEEE Trans. Aero. Electron. Sys.*, vol. 46, no. 2, pp. 745–760, Apr. 2010.

[43] A. M. Latham, R. Pilawa-Podgurski, K. M. Odame, and C. R. Sullivan, "Analysis and optimization of maximum power point tracking algorithms in the presence of noise," *IEEE Trans. Power Electron.*, vol. 28, no. 7, pp. 3479–3494, Jul. 2013.

[44] T. Esram and P. Chapman, "Comparison of photovoltaic array maximum power point tracking techniques,"

IEEE Trans. Energy Convers., vol. 22, no. 2, pp. 439–449, Jun. 2007.

[45] V. V. R. Scarpa, S. Buso, and G. Spiazzi, "Low-complexity mppt technique exploiting the pv module mpp locus characterization," *IEEE Trans. Ind. Electron*, vol. 56, no. 5, pp. 1531–1538, May. 2009.

[46] S. Kolesnik, M. Sitbon, S. Lineykin, E. Batzelis, S. Papathanassiou, T. Suntio, and A. Kuperman, "Solar irradiation independent expression for photovoltaic generator maximum power line," *IEEE J. Photovoltaics*, vol. 7, no. 5, pp. 1416–1420, Sep. 2017.

[47] X. Li, H. Wen, L. Jiang, W. Xiao, Y. Du, and C. Zhao, "An improved mppt method for pv system with fast-converging speed and zero oscillation," *IEEE Trans. Ind. Appl.*, vol. 52, no. 6, pp. 5051–5064, Nov. 2016.

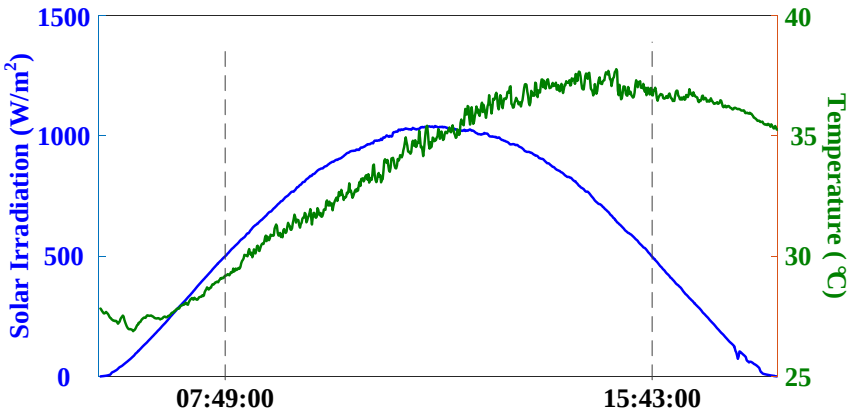

(a)

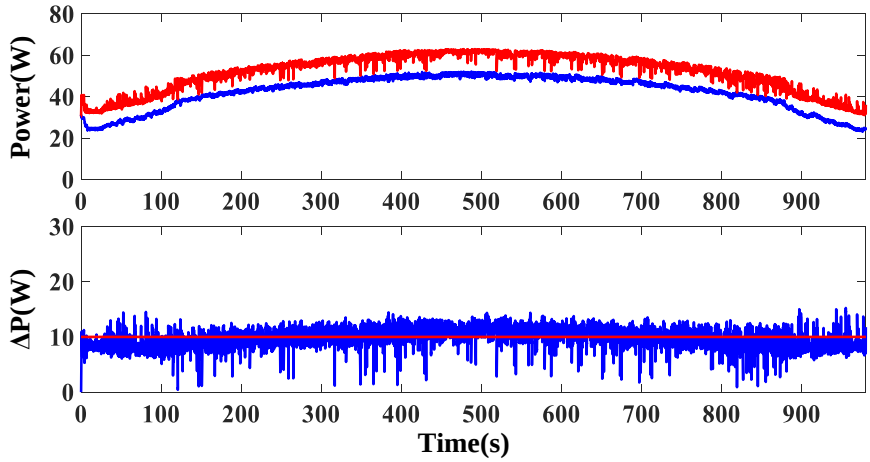

(b)

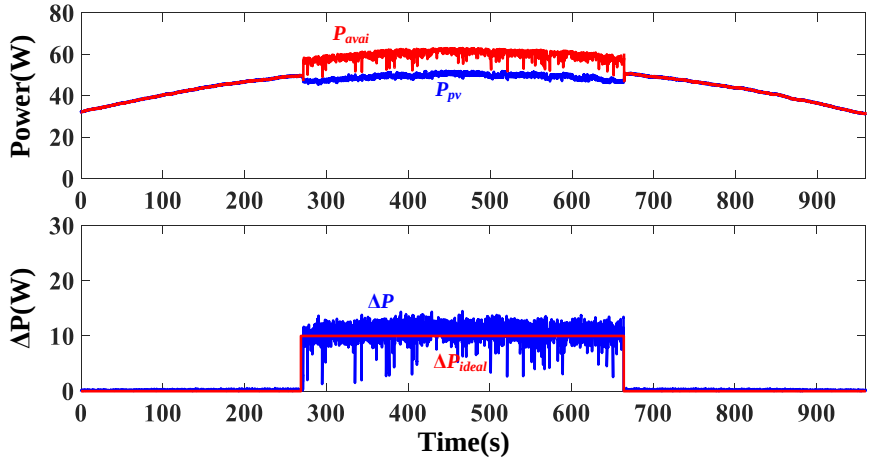

(c)

Fig. 19. Experimental results for the proposed control scheme under a clear day. (a) Solar irradiance and ambient temperature profiles in UNLV, Nevada, 24th Jul. 2015; (b) PRC mode with 10W reserved power is used in the whole process; (c) Both MPPT mode and RC mode with 10W reserved power are used.

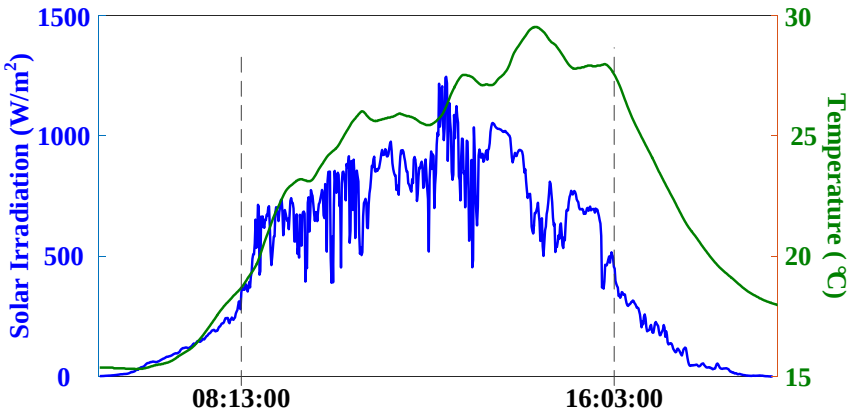

(a)

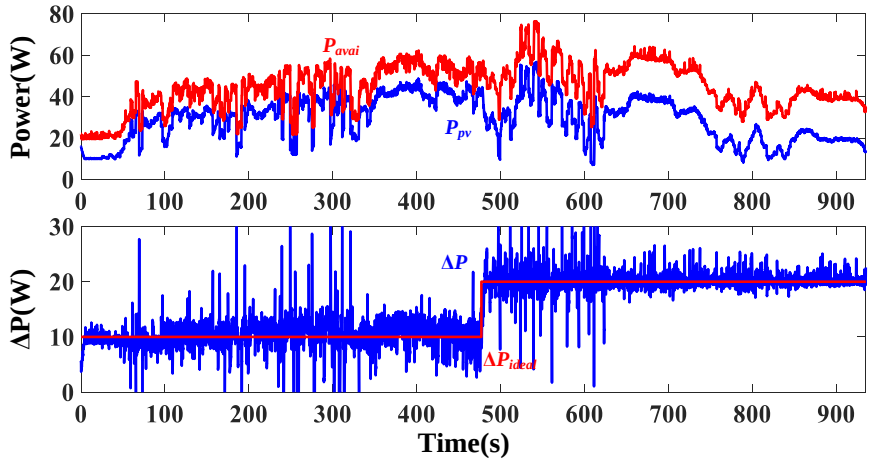

(b)

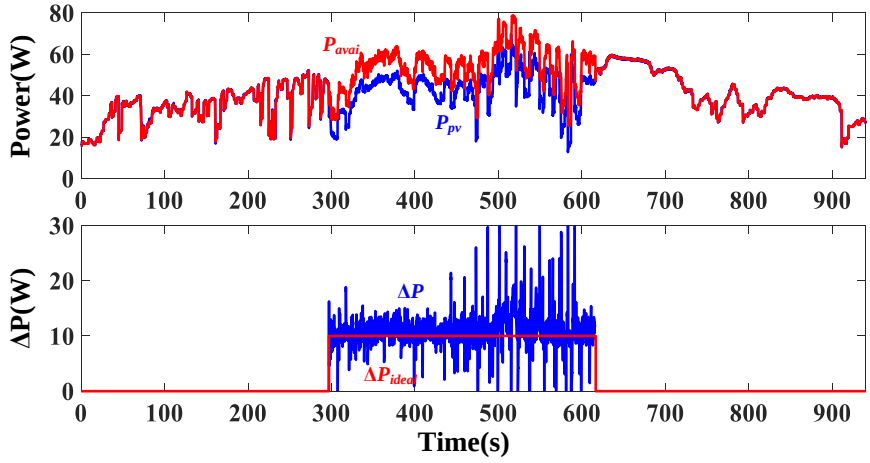

(c)

Fig. 20. Experimental results for the proposed control scheme under a cloudy day. (a) Solar irradiance and ambient temperature profiles in HSU, California, 31th Jul. 2015; (b) PRC mode with 10W and 20W reserved power are used; (c) Both MPPT mode and RC mode with 10W reserved power are used.